7.9

Evaluation of an Airborne Radar Turbulence Detection Algorithm

Larry B. Cornman, Shel Gerding, Greg Meymaris and John Williams

National Center for Atmospheric Research*
Research Applications Program
Boulder, CO

1. INTRODUCTION

Encounters with turbulence remains the leading cause of non-fatal accidents for large commercial transport aircraft. Statistics show that a significant number of these encounters are due to in-cloud and near-cloud turbulence. Many commercial aircraft are being fitted with windshear radars which also have the potential to detect convective turbulence. As part of NASA's Aviation Safety Program (AvSP), a joint industry-research community effort has been initiated to address this problem. This endeavor encompasses basic research into the phenomena, numerical modeling, the development of robust detection and quality control algorithms, end-to-end simulation and flight tests. The current operational goal for the airborne radar turbulence system is the detection of significant turbulence events, when the reflectivity is greater than 15 dBZ and with a lead time of 30-120 seconds.

Supporting the AvSP, the National Center for Atmospheric Research (NCAR) has developed a spectral level quality control algorithm and a turbulence detection algorithm. The quality control algorithm, the NCAR Efficient Spectral Processing Algorithm (NESPA), is a novel method for estimating Doppler moments and quality control indices (or *confidences*) for the moments. The turbulence hazard detection algorithm was jointly developed by NCAR and AeroTech Research (ATR), and takes the radar information and converts it into aircraft-specific hazard information.

In the following, brief discussions on NESPA and the turbulence hazard detection algorithm will be given. Results from NASA B757 flight tests and simulation will also be presented.

2. NESPA

NESPA is a method for determining Doppler moments and associated quality control values (confidences) from Doppler spectra. The method is novel in that is uses a multistage approach to finding moments from spectra to optimize the trade-off between processing capacity and accuracy. For real-time applications, a trade-off must be made between simplistic, yet computationally efficient moment generating methods (e.g., pulse pair algorithms) and more sophisticated, yet computational intensive methods (cf. Cornman, et. al.,1998). Typically, more sophisticated methods will yield more accurate moments. In NESPA, this trade-off is made iteratively, so that accuracy increases as available processing time increases. Furthermore, the important addition of confidences allows for an indication of the estimated quality of each moment – regardless of the number of iterations that are performed. Typically, as the number of iterations increases, the quality of the moments and the values of the confidences increase.

An important preprocessing step is the averaging (or median filtering) of the spectra. The importance of this step is discussed in Cornman, et. al. (1999, 2000). In the current implementation on the NASA B757, the spectra are averaged across azimuth, and median filtered along Doppler velocity and range.

3. TURBULENCE HAZARD DETECTION ALGORITHM

The goal of the turbulence hazard detection algorithm is to produce information that can be directly understood by the pilot. That is, the hazard information should not pertain to the state of the atmosphere, but rather to the effect that the turbulence will have on the aircraft. The hazard metric that is used is the standard deviation of the normal load on the aircraft, $\sigma_{\Delta n}$. The current methodology for estimating $\sigma_{\Delta n}$ at the spatial location $\underset{\sim}{r}$ (i.e., range, azimuth and elevation) is given mathematically by

$$\hat{\sigma}_{\Delta n}(\underset{\sim}{r}) = \left(\frac{\sigma_{\Delta n}}{\sigma_w}\right)\left(\frac{\sigma_u}{\langle M_2(\underset{\sim}{r})\rangle^{1/2}}\right)\langle M_2(\underset{\sim}{r})\rangle_{meas}^{1/2} \qquad (1)$$

where the two terms in brackets are theoretical calculations, $\langle M_2(\underset{\sim}{r})\rangle_{meas}^{1/2}$ is the square root of the average of Doppler second moments (generated by NESPA using averaged spectra), and $\hat{\sigma}_{\Delta n}$ is the estimate for $\sigma_{\Delta n}$.

In the calculation of the terms in brackets, the assumption of a von Karman, isotropic wind field model with an integral length scale of 500 m has been made. The first term in brackets deals with the standard deviation of thenormal load response of the aircraft, per unit standard deviation of the vertical component of the turbulent wind field. This requires a knowledge of specific state of the given aircraft, i.e., weight, altitude, true airspeed and of course, the response of the aircraft in this

Corresponding author address: Larry B. Cornman
National Center for Atmospheric Research
Research Applications Program, P.O. Box 3000,
Boulder, CO, 80307-3000, E-mail: cornman@ucar.edu

*The National Center for Atmospheric Research is sponsored by the National Science Foundation.

state. The NASA B757 response values were calculated via data obtained from the NASA aircraft simulator. The second term in brackets relates the (inverse of the) square root of the averaged second moments (generated by averaging spectra), to the standard deviation of the u-component of the wind field (assuming the radar is pointing along the x-axis). The mathematics of this calculation is described in Cornman, et. al. (2000). (Note that the last two pages of that paper were cut-off.)

4. RESULTS FROM NASA FLIGHT EXPERIMENT

During Fall 2000, a set of flight tests using the NASA B757 were conducted. A description of these flights is given in Hamilton and Proctor (2002). The radar was a standard airborne windshear radar, modified to record raw I and Q data. The aircraft had a relatively high quality air data system for making *in situ* wind and turbulence measurements.

The averaged spectra generated from the I and Q data were processed and run through NESPA and the turbulence hazard detection algorithm. Comparisons between these hazard values and the measured aircraft values were made. The radar operated in two modes, a standard weather sweep (long pulse mode, for the pilot's reflectivity display), and "hazard" sweeps (short pulse mode). The hazard sweeps consisted of three elevation tilts, 0, -2 and -4 degrees. The time interval between the completion of the three elevation sweeps and the next set was on the order of 12 s. The hazard values as given by Eq. (1) for a given pulse volume were then processed over the three elevation scans to give a final hazard value. This was given by the (confidence-weighted) 90th percentile hazard value over a 5x5x3 (range, azimuth, elevation) set of pulse volumes. Hence, the final hazard product over the three elevations consists of one number at each range and azimuth -- assigned to the zero degree elevation. Fig. 1 illustrates this hazard product for event 191-06, at time 18:43:46 GMT. Overlaid on the radar product is the flight track of the aircraft, with the aircraft measured hazard value, updated every five seconds, or approximately 1.2 km for the airspeed in this case.

For each radar/aircraft hazard field (as in Fig. 1), the value at each aircraft update was compared to local statistics of the radar field. For example, the radar hazard values in a 1-km disc around the aircraft value would be processed to give the minimum, maximum and median hazard value over the disc. It should be noted that for a fixed disc, the number of radar hazard samples will decrease as a function of increasing range. Another option was to use a fixed number of ranges and azimuths surrounding the aircraft sample.

Table 1 is a contingency table for seven flight segments, using the one km disc method described above, and the radar hazard value used for comparison was the median value over the disc. The hazard thresholds relate to moderate turbulence. Note that this comparison method results in many partially dependent samples. That is, for each given time many of the spatial regions (1 km discs) are highly overlapping. Furthermore, as the radar hazard values update every 12 s, and the atmosphere is somewhat stationary over that temporal regime, the same turbulent "event" may be sampled more than once.

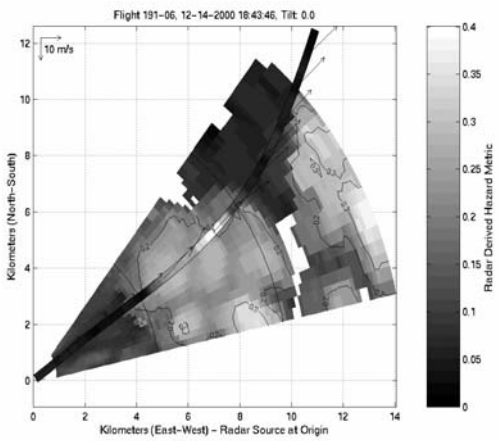

Fig. 1 Radar and aircraft hazard values for flight 191-06

		Aircraft Hazard ≥ 0.2	Aircraft Hazard < .2
Radar Hazard	≥ 0.2	**70**	**12**
	< .2	**368**	**9257**

Table 1: Contingency Table for 1 km disc.

For these flights, the POD was 0.16, FAR 0.15, and CSI 0.16. Clearly, the problem is mainly related to missed detections, not false alerting. Half of the false detections were in flight 181-07, the other half in 191-06. Half of all the missed detections were in 190-4 and 190-06. All correct detections were in 191-06. The percent of aircraft values between minimum and maximum of the radar values was 46%, however it should be noted that most of these discrepancies occurred in three long flight segments. In the three 191 flight segments (about 25% of the total samples), significant turbulence events occured and the percent between min. and max values was over 70%. A histogram of the differences between the radar and aircraft hazard values, showing the propensity for underestimation, is given in Fig. 2.

The few false detections were due to two distinct issues. On one flight, the aircraft was making a significant turn, such that the aircraft track went though the edge of the radar domain. Due to the motion of the aircraft, and hence apparent wind perpendicular to the pulse volume, a non-trivial amount of Doppler second moment results. This problem is exacerbated when the spectra are averaged, as was the case for these data. The false detections in this case occurred when the first-cut correction factor did not remove enough of the contaminating second moment. The other false detections were due to slight misalignment of the radar and aircraft hazard detections. Fig. 3 shows an example of this problem (at the lead-in to the event) for flight segment 191-06. The asterisks indicate the median value of the radar hazard values

over the disc and the dashed lines indicate the minimum and maximum values.

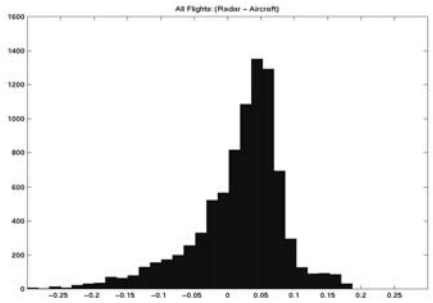

Fig. 2 Histogram of radar - aircraft hazard differences.

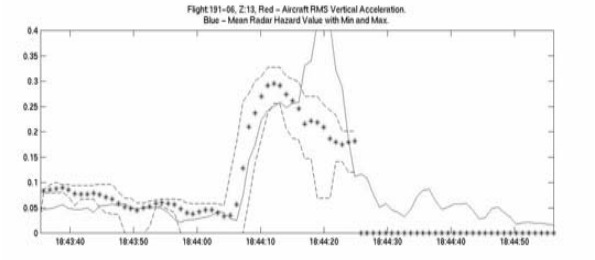

Fig. 3 Comparison of radar and aircraft hazard values

One source of missed detections is again the misalignment problem, and is seen in Fig. 3 at the tail end of the event. Nevertheless, the most significant problem with missed detections was due to anisotropy in the turbulent wind field. The aircraft normal load is dominated by the response to vertical wind variations. On the other hand, the radar measurables (first and second Doppler moments) only give information related to velocities along the radar line-of-sight, i.e., approximately perpendicular to the vertical velocities. In vigorous thunderstorms, it is natural to expect that large updraft/downdraft regions would create turbulence, which at its onset (i.e., prior to significant mixing), would have a predominant amount of energy in the vertical direction. Fig. 4 shows a clear example of this anisotropy. The top panel in the figure shows the standard deviations of the along-track and vertical wind components. The lower panel shows the standard deviations of the normal load on the aircraft. All standard deviations were calculated over 5 s (1.2-km) regions. The large relative increase in σ_w at the end of time sequence -- just as the normal load peaks -- shows how the radar can miss a detection for anisotropic wind fields. Note that the factor of two between the σ_w and σ_u values around the "big hit" in Fig. 4 is similar to the ratio in the aircraft and radar hazard values seen in Fig. 3.

In summary, the results from the initial NESPA and hazard detection algorithms are somewhat mixed. From the operational viewpoint, minimizing false detections is a critical concern and hence the algorithms performed very well. Nevertheless, the missed detections are still problematic. On the other hand, the scoring rules used in the analysis given above were fairly stringent. As can be seen from Fig. 1 and Fig. 2, the radar algorithm would have given an operationally-useful warning for the 191-06 case. In fact, of the seven flight segments analyzed, there were only a couple of events that were missed entirely. These were very short duration encounters with convective plumes (flight 190, see Hamilton and Proctor, 2002) and hence the anisotropy was a dominant factor in these missed detections. In the future, information from the first moment fields will be examined to see what benefit it might provide to the detection problem.

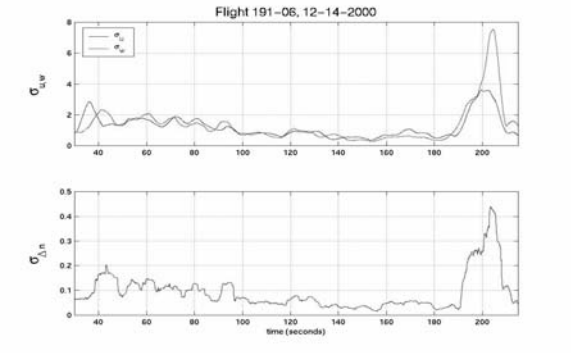

Fig. 4 Time history of σ_u and σ_w (upper panel) and $\sigma_{\Delta n}$ (lower panel), for flight segment 191-06.

5. RESULTS FROM SIMULATION

An extremely valuable tool for the development and analysis of algorithms is simulation. NCAR has developed a radar simulation package that takes in gridded wind and reflectivity fields and outputs I & Q time series. Two methods are available to produce the input wind fields, a stand-alone isotropic von Karman wind field generator and a combined cloud-scale model with embedded "sub-grid" turbulence. In the following, the second method will be discussed (the first method is used in the second).

A samall set of cloud-scale model simulations are being used in the NASA program, one of which is the 191-06 case discussed above. A description of this simulation is given in Proctor and Hamiltion (2002). This cloud-scale model was run to a 100-m grid spacing. Due to the inherent filtering in the model, the actual resolved scales were on the order of 800 m. Unfortunately, the scales of motion that are pertinent for both the radar and aircraft problem are on the order of 25-500 m. Of course, the cloud-scale model could be run at smaller grid spacing, but since the total number of grid points is a computational restriction, this would result in physical domains which are too small for the radar simulation problem. Therefore, a method was developed to merge a sub-grid turbulence wind field with the cloud-scale field.

First, the 100-m cloud model data was interpolated to a 25 m grid, then the turbulent subgrid wind fields (as computed using the von Karman algorithm described in Frehlich et. al., 2001), were added component-by component. The von Karman subgrid parameters (variance and outer length scale) were determined from a best fit of the model generated structure functions (after interpolation) to the desired Kolmogorov behavior (i.e. 2/3 slope). When

merging the subgrid winds with the interpolated cloud model winds, the amplitude of the subgrid winds was spatially modulated by the square root of the structure function computed at lag 28 from the interpolated cloud model data. The reflectivity from the cloud-scale model was merely interpolated to the 25 m grid.

Fig. 5 shows the reflectivity field from the cloud-scale model, interpolated to the 25 m grid. The white dot at the lower right is the location of the radar for the simulation and the white outlined area is the domain for the simulation. This region corresponds to the "big hit" illustrated for the 191-06 flight segment, above. Note that the simulation domain is oriented relative to the large-scale thunderstorm line within which this event was located, whereas the data shown above (e.g., Fig. 1) is referenced to the actual N-S, E-W coordinates.

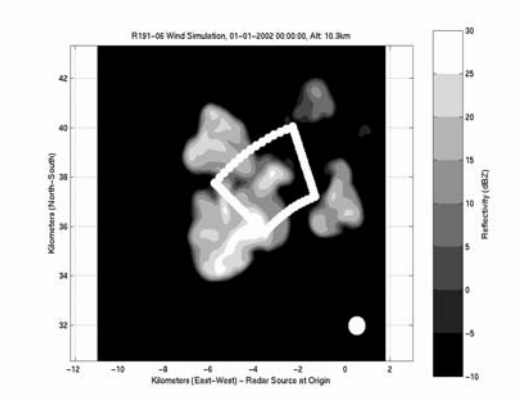

Fig. 5 Reflectivity field for the 191-06 simulation

The hazard values from the radar simulation are shown in Fig. 6. The "aircraft" hazard overlay was generated using

$$\hat{\sigma}_{\Delta n}(\underset{\sim}{r}) = \left(\frac{\sigma_{\Delta n}}{\sigma_w}\right)\sigma_w(\underset{\sim}{r})_{meas}, \qquad (2)$$

where the term in brackets is the same such term in Eq. (1) and the measured $\sigma_w(\underset{\sim}{r})$ value is given by the standard deviation of the w-component of the wind field, over 1x1 km squares, in the horizontal plane. The results from the simulation are quite similar to those seen in the real case. In fact, the same underestimation of the event due to anisotropy is visible in Fig. 6. Fig. 7 shows a spatial series of standard deviations of the vertical component and the component of the wind along the "aircraft track." Via the Doppler second moment, the radar hazard values are proportional to the along-track variances.

An advantage of using simulation to investigate algorithm performance is that many "flight paths" can be investigated with one cloud-scale/sub-grid simulation.

6. SUMMARY

Great strides have been made in the NASA AvSP turbulence activity, including algorithm development, flight experiments, understanding convective turbulence characteristics, radar and turbulence simulation. There is more work to be done, but the potential of using airborne Doppler radars to detect convective turbulence is clear.

7. ACKNOWLEDGEMENT

This research was sponsored by NASA's Aviation Safety Program.

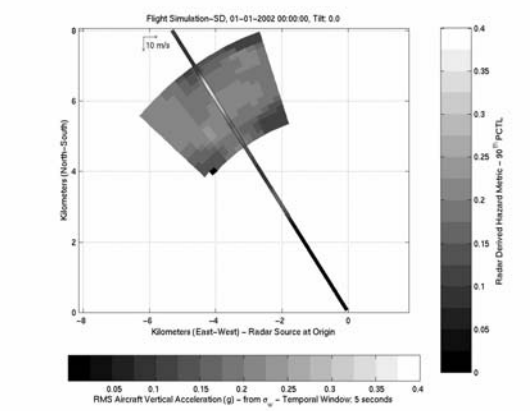

Fig. 6 Radar and "aircraft" hazard values for the 191-06 simulation.

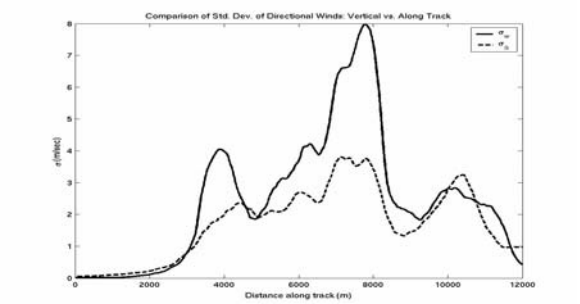

Fig. 7 Spatial series of σ_a and σ_w along the simulated flight segment.

8. REFERENCES

Cornman, L.B., R. Goodrich, C. Morse and W. Ecklund, 1998: A fuzzy logic method for improved moment estimation from Doppler spectra, *J. Atmos. Oceanic Technol.* **15**, 1287-1305.

Cornman, L.B., R. Goodrich, R. Frehlich, B. Sharman and N. Beagley, 1999: The detection of convective turbulence from airborne Doppler radars, Preprints, 29th International Conference on Radar Meteorology, 12-16 July, Montreal, Amer. Meteor. Soc. 864-867.

Cornman, L.B., J. Williams and R. Goodrich, 2000:The detection of convective turbulence using airborne Doppler radars, Preprints, 9th Conference on Aviation, Space and Aerospace Meteorology, 11-15 September, Orlando, Amer. Meteor. Soc., 569-572.

Frehlich, R., L. Cornman and R. Sharman, 2001: Simulation of three-dimensional turbulent velocity fields, *J. Appl. Met.*, **40**, 246-257.

Hamilton, D.W. and F. Proctor, 2002: Meteorology associated with turbulence encounters during NASA's Fall-2000 flight experiments, Paper AIAA 2002-0943, 40th Aerospace Sciences Meeting and Exhibit, 14-17 January, Reno, NV.

Proctor, F.H. and D. Hamilton, 2002: Numerical study of a convective turbulence encounter, Paper AIAA 2002-0944, 40th Aerospace Sciences Meeting and Exhibit, 14-17 January, Reno, NV.